Biotribology 18 (2019) 100097

Contents lists available at ScienceDirect

Biotribology

journal homepage: www.elsevier.com/locate/biotri

An Empirical Approach for the Determination of Skin Elasticity: Finger pad Friction against Textured Surfaces

D.A. Sergachev[a,*], D.T.A. Matthews[a], E. van der Heide[a,b,c]

[a] Laboratory for Surface Technology and Tribology, Faculty of Engineering Technology, University of Twente, Enschede, the Netherlands.
[b] Delft University of Technology, Faculty of Civil Engineering and Geosciences, Railway Engineering, Delft, the Netherlands.
[c] Ghent University, Faculty of Engineering and Architecture, Labo Soete, Ghent, Belgium

ARTICLE INFO

Keywords:
Skin tribology
Tactile friction
Young's modulus
Surface texture

ABSTRACT

Surface topography significantly influences tactile friction and perception. While friction forces can be reduced by surface texturing, selection of pattern dimensions is challenging due to the highly variable elastic modulus of the skin. This work proposes an empirical approach for the evaluation of the skin elasticity through surface transition from asperity to full contact state. To highlight the contact transition, two textures with evenly distributed identical micro asperities, but varying density, were moulded with several grades of silicone rubber. Dynamic friction coefficient measurements were performed during finger pad sliding against the textured samples with a range of normal loads up to 5 N. A combination of analytical and numerical contact models is used to explain the observed friction behaviour, estimate the development of contact area and calculate the effective elastic modulus of the skin at the micro-scale. Low density textures clearly indicate the transition to the full contact state, which is reflected in friction coefficient development, while high density textures remain in an asperity contact state, with significantly lower friction values. The effective Young's modulus is hereby estimated in the range of 0.2–0.5 MPa. Observed frictional behaviour is explained by the change in the apparent and real contact areas. The presented approach allows to study the influence of individual surface parameters on effective skin elastic modulus, which is essential for the development of functional surfaces with improved tactile perception.

1. Introduction

Touch is one of the main senses that provides information for object perception. Tactile exploration, for example, allows object shape, edges and texture to be determined through mechanoreceptors located in the skin. Perceived surface feel is generally divided into three categories: hardness, roughness and stickiness [1], where the last two have been reported to be related to the topographical structure. Indeed, Skedung et al. [2] reported a positive relationship between perceived coarseness and surface roughness and stickiness feel was found to correlate with friction coefficients [3]. Moreover, surface discrimination was found to be influenced by surface texture to fingerprint wavelength ratio, which defines the induced vibrations during tactile exploration [4,5]. However, the overall understanding of touch and touch perception is not yet robust.

While haptic perception varies between individuals, it relies on the forces experienced during touch [6]. Friction forces arising from a finger pad sliding over a surface can be approximated by a two-term model, which describes the friction as a sum of the interfacial adhesion and deformation components [7,8]:

$$F_{tot} = F_{adh} + F_{def} \quad (1)$$

In dry sliding against smooth surfaces, the adhesion term is predominant [9–11], however, with an increase of the surface roughness and asperity heights, the deformation component increases. Tomlinson et al. [12] observed a rise in the friction coefficient with increase of the machined roughness up to a certain point, after which it plateaued. For the triangular ridged surfaces with a height of 250 μm the deformation term reached 10% of the total friction [13]. Moreover, a considerable influence of the interlocking friction component was reported, which became predominant at the ridge heights above 42.5 μm. Darden et al. [14] studied a sliding contact against spherical bumps with heights of 0.48, 0.75 and 1.0 mm. Interaction with a bump was separated from background signal as a differential friction coefficient for analysis. It was concluded that hysteretic deformation of the finger pad was the dominant mechanism in the observed rise of friction.

* Corresponding author.
E-mail address: d.sergachev@utwente.nl (D.A. Sergachev).

https://doi.org/10.1016/j.biotri.2019.100097
Received 15 November 2018; Received in revised form 9 April 2019; Accepted 8 May 2019
Available online 11 May 2019

Nomenclature

A_a	apparent contact area of a finger pad, measured with a fingerprint scannerm^2
a_{ac}	equivalent radius of an apparent contact area, calculated for an elastic materialm
A_{ac}	apparent contact area of a finger pad, calculated for an elastic materialm^2
a_g	equivalent radius of a gross finger pad contact aream
A_g	gross contact area of a finger pad, measured with a fingerprint scannerm^2
a_{gc}	equivalent radius of a gross finger pad contact area, calculated for an elastic materialm
A_{gc}	gross contact area of a finger pad, calculated for an elastic materialm^2
A_r	real contact aream^2
a_{trans}	equivalent radius of an apparent contact area in a full contact statem
A_{trans}	apparent contact area in a full contact statem^2
E_0^*	effective Young's modulus in macro contactPa
E_1^*	effective Young's modulus in micro contactPa
E_{fp}	Young's modulus of a finger padPa
E_m	Young's modulus of a material samplePa
E_{smc}	effective skin Young's modulus in micro-scale contactPa
F	applied normal loadN
F_{adh}	interfacial adhesion friction forceN
F_{crit}	normal load at which a transition to a full contact state occursN
F_{def}	hysteresis friction forceN
$\overline{F_i}$	mean force acting on individual asperityN
$F_{i\ crit}$	critical force acting on individual asperity at which a transition to a full contact state occursN
$F_{i\ max}$	maximum force acting on individual asperityN
F_{tot}	total friction forceN
h_{asp}	height of an asperitym
k	power-law coefficient for contact aream^{2}N^{-m}
k_a	power-law coefficient for apparent contact aream^{2}N$^{-m_a}$
k_g	power-law coefficient for gross contact aream^{2}N$^{-m_g}$
m	power-law load index for contact area–
m_a	power-law load index for apparent contact area–
m_g	power-law load index for gross contact area–
N	number of texture asperities in contact–
$\overline{p}$	mean apparent contact pressurePa
$p(r)$	finger pad pressure radial distributionPa
$\overline{p}_{asp}$	mean apparent contact pressure in an asperity contact state areaPa
$\overline{p}_{crit}$	critical apparent contact pressure at which a transition to a full contact state occursPa
p_{max}	maximum apparent contact pressurePa
$\overline{p}_r$	mean real contact pressurePa
$\overline{p}_{trans}$	mean apparent contact pressure in a full contact state areaPa
r	radial distance from contact centrem
R_{asp}	radius of an asperity tipm
R_e	equivalent radius of a finger padm
α	pressure coefficient–
β	viscoelastic hysteresis loss fraction–
δ	total micro-displacement of contacting surfacesm
λ	spacing between texture asperitiesm
μ_{adh}	interfacial adhesion coefficient of friction component–
μ_{def}	hysteresis coefficient of friction component–
μ_{tot}	total coefficient of friction–
τ	interfacial shear strengthPa
τ_0	intrinsic interfacial shear strengthPa
υ_{fp}	Poisson's ratio of a finger pad–
υ_m	Poisson's ratio of a sample material–
υ_{smc}	Poisson's ratio of skin in micro-scale contact–

As long as the adhesion term prevails, friction directly correlates to the real contact area. Therefore, a separation of the contacting bodies, caused by initial increase in the surface roughness, leads to a decrease in the friction coefficient for the dry skin contact [9,15,16]. Moreover, tactile friction can be controlled by deterministic roughness produced by surface structuring. Van Kuilenburg et al. [17,18] tested micro-textured surfaces with spherical tips of different radii and spacing, thus reducing real contact area and the observed friction values. It was concluded that a minimum value for the coefficient of friction can be achieved, before deformation and interlocking friction becomes predominant. Finding optimal texture dimensions to minimize skin friction is not a trivial task. The required surface geometry varies with the manufacturing process limitations, material properties of a product and its application conditions, given the system dependence of friction.

Mechanical properties of the skin vary due to its anisotropic structure and responsive behaviour to the changes in the environment. Finger pad stratum corneum (SC), the outer layer of the epidermis, is comprised of corneocytes [19] with the thickness varying between 200 and 350 μm [20–22]. This is much higher than the SC in other anatomical locations, where it is usually observed in the range of 10–40 μm [23–25]. While asperity height is significantly lower than stratum corneum layer thickness, micro-scale skin deformation and development of the real contact area is expected to depend mostly on the elastic properties of the SC. Indentation measurements to study the Young's modulus of SC are usually performed on the volar forearm skin, where hair is not present, and the skin has uniform structure with relatively low roughness. Mechanical properties of the finger pad skin are harder to evaluate due to the curvature and periodic ridge structure. Furthermore, a measured effective elastic modulus heavily depends on indenter size and skin displacement due to the underlying softer dermis layer [26,27]. Abdouni et al. [28] used a glass indenter with a curvature of 2.5 mm and an air blast system to measure the finger pad elastic moduli *in-vivo*, which was found to be in the range between 10 and 100 kPa. Similar effective elastic modulus of 70 ± 20 kPa was observed by P. Cornuault et al. [29]. *In-vitro* SC indentation measurements provide dramatically higher values in the range from 1 MPa to 1 GPa [23–25]. It remains unclear what skin elastic modulus should be used for the surface texture design and how it scales with individual asperity dimensions.

The aim of the current work is to use a contact transition, from an asperity-only to a full contact state, as a cue to estimate skin Young's modulus at the micro-scale. The contact state is detected through friction measurements of a finger pad sliding against textured surfaces. After the point of transition, the real contact area of the skin is expected to escalate, thus leading to the increase in the observed friction coefficient. While such effect was discussed by other researchers [18,30,31], its development with normal load was not shown experimentally. At the point of transition, a combined micro displacement of the asperities and the skin equals the asperity height. Therefore, the skin elastic modulus can be calculated, if the applied forces and the counter-material properties are known. Moreover, by using multiple rubber grades with similar surface energy but various hardness, interfacial shear strength remains relatively similar, while the relative asperity displacement is varied; consequently, the asperity normal loads required for the contact transition to happen are modified. While the normal forces applied to asperities are inversely proportional to the apparent contact area, adding varying material properties to the sample matrix allows for comparison of relative changes in the fingerprint

ridge contact area and the contact model accuracy improvement. Observations of the micro-contact behaviour will allow to optimise surface texture dimensions and predict finger pad friction.

2. Materials and Methods

2.1. Materials

A total number of twelve samples were studied in this work: two surfaces with a textured area of 50 × 50 mm and a non-textured reference, each reproduced in a series of four various silicon rubber grades. Both textures consist of evenly distributed square packed asperities with an average asperity tip radius of 19 ± 3 μm and a height of 28 ± 2 μm. The patterns differ in the asperity density created by asperity lateral spacings of 100 and 200 μm (Fig. 1). The surface topography of the samples was measured using a 3D LED confocal microscope S neox (Sensofar, Spain).

Negative textures were produced by laser ablation on a stainless spring steel sheet, from which textured master samples were created in a silicone rubber by moulding. The master samples were replicated by a double moulding technique using polyurethane resin Smooth-Cast® 305 (Smooth-on, USA) for a negative mold. This intermediate step was used to reduce the adhesion during separation and improve reproducibility of the micro-texture dimensions. The samples were moulded with constant thickness of 10 mm in various hardness grades using commercially available tin cure silicone rubber Mold Max™ (Smooth-on, USA), further abbreviated by letter M followed with elastomer respective Shore A hardness. Rubber elastic moduli were estimated from the materials' technical datasheets and presented in the Table 1 along with the measured texture dimensions of the tested surfaces.

2.2. Friction Measurements

Experiments were performed *in-vivo* on a dedicated setup designed by Klaassen et al. [32]. The test rig was adapted for the finger pad friction measurements and consists of an enclosed chamber with a linear reciprocating tribometer (Fig. 2). The right hand is placed on a stage with an index finger inclination angle of 30 degrees relative to the sample. A transducer is mounted on the mechanical hinge and the normal load is applied with static weights. The samples were glued to polymethyl methacrylate (PMMA) plates, which were fastened to the load cell by bolt fixture. The sample textures were aligned parallel to the sliding direction.

Friction measurements were conducted with a constant sliding velocity of 2 mm/s and a stroke length of 20 mm. Acceleration was set to 2 mm/s^2 so it did not influence the dynamic coefficient of friction. The load cell was moving from the subject body, thus simulating the usually performed backward finger pad friction experiments. After each measurement the hinge was lifted, and the carriage was returned to the starting position.

The samples were tested with a large array of normal loads to detect the changes in friction coefficient with high precision. The low loads region, where adhesion friction component remains predominant, was of particular interest. Therefore, each sample was measured under 19 normal loads: from 0.1 to 0.6 N with a step of 0.1 N, from 0.6 to 2 N with a step of 0.2 N and from 2 to 5 N with a step of 0.5 N. Normal load was applied for 5 s before the motor movement was initiated. Three consecutive measurements were performed per each applied normal load.

Given the test matrix, the experimental part was split into separate measurement series and was carried out on different days. Each test series included four samples with the same representative surface but various rubber grades. The samples were tested consecutively with increasing normal load. However, the above approach means that the tests were not fully randomized - in part due to the size of the test matrix and in part due to concerns of the possible texture wear and, therefore, change of the contact conditions. This is acknowledged as a limitation of the work presented. That said, all environmental conditions are reported below, and their effects are considered in section 4.

Prior to the measurements the samples were cleaned with acetone-moistened and alcohol-moistened tissues, rinsed with demineralized water and kept in a vacuum chamber for 12 h prior to the experiment to prevent possible rubber swelling.

Experiments were carried out in ambient environmental conditions, which are presented in Table 2. The hands were washed with soap and dried in air for 15 min before friction measurements against each sample. Skin hydration of the index finger pad was monitored with Corneometer CM 825 (Courage + Khazaka GmbH, Germany) to ensure that moisture content remained relatively stable between testing various sample materials. The average hydration level of the skin remained at 55 ± 7 AU, which corresponds to the normal skin hydration level [33].

2.3. Apparent Contact Area Measurements

Gross and apparent contact areas of the tested index finger pad were measured with a digital fingerprint scanner FS50 (Futronic Technology Co. Ltd., China) during sliding. Inclination angle and sliding velocity were controlled manually and were kept similar to the ones used in the friction measurements. Obtained images were filtered by histogram equalization and converted into a binary image by setting a threshold value [31,34], which is further described in the supplementary material. The total number of pixels from the binary image was multiplied by a scanner resolution to calculate apparent contact areas. Gross contact area was calculated from the best ellipse fit to the image. The images were scanned horizontally to detect dark to bright transition points. The obtained point arrays were used for the best oval fit function.

2.4. Data Processing

The normal and friction forces were measured using a 6-axis Mini40 transducer (Schunk, Germany) with a sampling rate of 100 Hz. The load cell has a resolution of 6 mN in the normal direction and 2 mN in the tangential direction.

In this work we differentiate the friction coefficient as measured during the whole test from the relevant dynamic friction coefficient using a Matlab code. Succinctly put, this is a stable region after the first local maximum of a high order polynomial fit (Fig. 3). The reason for doing this is to ensure that the initial slope, which corresponds to the elastic deformation before relative sliding motion starts, does not affect the average values. The friction measurements performed at normal load of 0.1 N were filtered manually due to the high deviations in the friction coefficient curve.

Moreover, a high wavelength noise was induced to the measurements by the guide bearing, which corresponds to the pitch distance

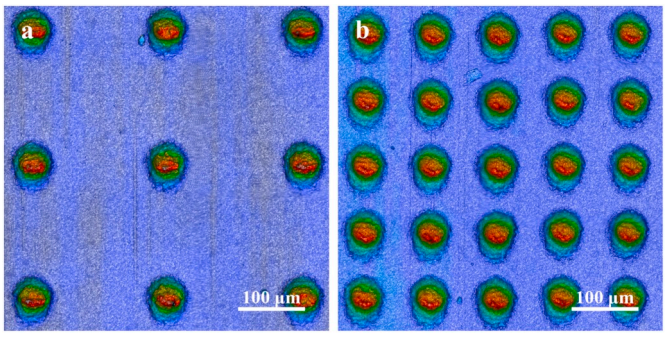

Fig. 1. Confocal images of the produced sample textures with asperity spacing of 200 μm (a) and 100 μm (b).

Table 1
Measured sample texture dimensions, average roughness and silicone rubber grades.

Sample texture	Sample material	Asperity tip radius, R_{asp} [μm]	Asperity height, h_{asp} [μm]	Asperity lateral spacing, λ [μm]	Average roughness, S_a [μm]	Shore A hardness, [−]	Estimated Young's modulus, E_m [MPa]
Flat ref.	M10	–	–	–	0.059	10	0.20
	M30	–	–	–	0.035	30	0.75
	M40	–	–	–	0.022	40	1.30
	M60	–	–	–	0.056	60	2.30
L200	M10	18.8 ± 1.9	27.9 ± 1.1	200	1.85	10	0.20
	M30	18.8 ± 0.8	28.9 ± 0.8	200	1.83	30	0.75
	M40	18.4 ± 0.5	28.8 ± 0.3	200	1.97	40	1.30
	M60	18.4 ± 1.9	27.1 ± 0.9	200	1.96	60	2.30
L100	M10	20.4 ± 1.3	27.7 ± 0.6	100	4.73	10	0.20
	M30	20.1 ± 0.8	28.1 ± 0.6	100	4.89	30	0.75
	M40	19.7 ± 1.2	28.3 ± 0.4	100	5.57	40	1.30
	M60	19.9 ± 0.9	28.0 ± 0.4	100	5.85	60	2.30

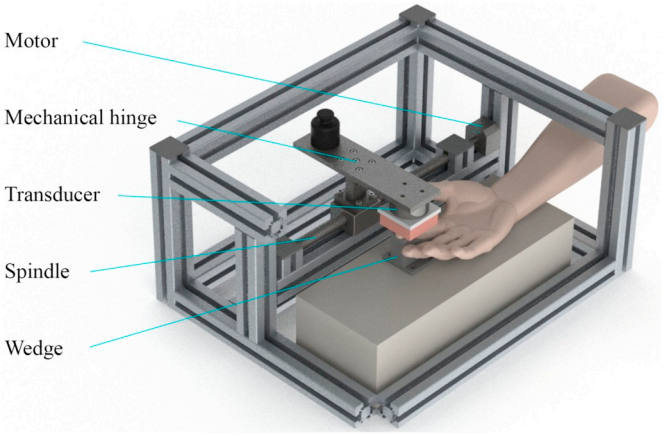

Fig. 2. Schematic representation of the test setup used for the friction measurements.

Table 2
Humidity and temperature during measurements.

	Flat reference	L100	L200	Fingerprint area measurements
Humidity [%]	63 ± 5	42 ± 3	56 ± 4	55
Temperature [°C]	24 ± 1	23 ± 1	24.5 ± 1	23

and the number of complete shaft revolutions. Therefore, the sine component with a frequency of 0.5 Hz was removed to reduce signal deviations, also by a Matlab script. A sine wave with a given frequency was fitted to find an amplitude and a phase offset for each measurement. Those values were used to subtract a corresponding sine function from the original signal. Inclination of the signal remained unchanged to ensure that filtering will not influence average friction values, but only reduce the standard deviation caused by induced signal noise.

3. Calculation

3.1. Apparent Contact Area

Considering a relatively soft sample material, a measured gross contact area must be corrected for the sample elasticity. Based on the Hertzian contact theory the elastic modulus of the finger pad E_{fp} can be estimated from the fingerprint scanner measurements as [35]:

$$E_{fp} = \frac{3}{4}\frac{FR_e}{a_g^3}(1 - \upsilon_{fp}^2), \tag{2}$$

where R_e and υ_{fp} are an equivalent radius and Poisson's ratio of the finger pad respectively and a_g is an equivalent radius of the measured gross contact area. Therefore, the corrected gross contact area Agc can be described as:

$$A_{gc} = \left(\frac{3}{4}\frac{FR_e}{E_0^*}\right)^{\frac{2}{3}}, \tag{3}$$

with a reduced elastic modulus $E_0{}^* = 1/((1 - \upsilon_{fp}{}^2)/E_{fp} + (1 - \upsilon_m{}^2)/E_m)$, where υ_m and E_m are a Poisson's ratio and a Young's modulus of the tested material. Assuming that apparent to gross contact area ratio remains the same at a given normal load as measured A_a/A_g, the new corrected ridge contact area A_{ac} can be calculated as:

$$A_{ac} = A_{gc}A_a/A_g \tag{4}$$

The number of micro asperities in contact with the finger N is calculated from the lateral spacing of the features λ as [17]:

$$N = A_{ac}/\lambda^2 \tag{5}$$

Therefore, the mean normal force acting on the individual asperity $\overline{F_i}$ can be expressed through normal load or mean apparent pressure $\overline{p}$ as:

$$\overline{F_i} = F/N = \overline{p}\,\lambda^2 \tag{6}$$

3.2. Pressure Distribution

The largest local skin displacement occurs in the region of maximum pressure, where local normal loads are the highest. Assuming a Hertzian spherical pressure distribution and a corresponding ratio $p_{max}/\overline{p}$ of 1.5, the maximum forces per asperity can be calculated as $F_{i_{max}} = 1.5 * \overline{F_i}$.

For the defined asperity geometry, the combined micro displacement of the skin stratum corneum layer and individual asperity will reach asperity height at an unknown force per asperity $F_{i_{crit}}$ and a corresponding mean apparent pressure $\overline{p}_{crit}$. It leads to the transition from asperity-only to full surface contact. With an apparent contact area equivalent radius a_{ac} the part of the apparent contact area in transition can be found from Hertzian spherical pressure distribution:

$$p(r) = \frac{3}{2}\overline{p}\sqrt{1 - \frac{r^2}{a_{ac}^2}} \tag{7}$$

Substituting the radii and pressure in the expression, it can be rewritten for the transition case as:

$$F_{i_{crit}} = \frac{3}{2}\overline{F_i}\sqrt{1 - \frac{A_{trans}}{A_{ac}}}, \tag{8}$$

where A_{trans} is an apparent contact area in the full contact state. Therefore, the ratio of the deformed-to-apparent contact area can be

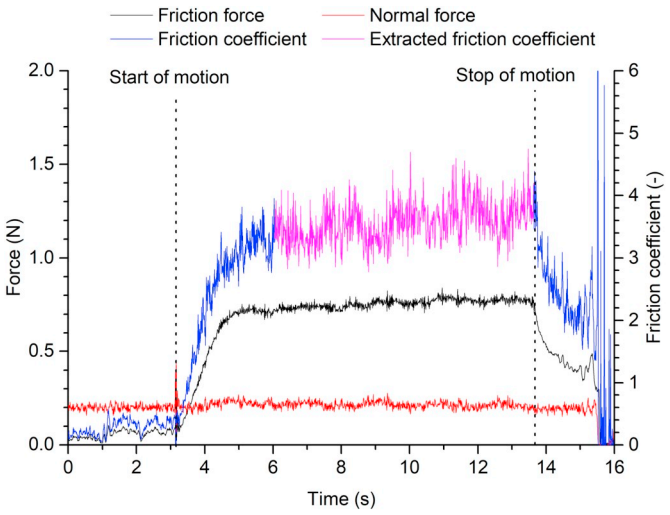

Fig. 3. Raw force signals with calculated and extracted dynamic friction coefficient. Non-textured M60 sample at 0.2 N normal load.

calculated as:

$$\frac{A_{trans}}{A_{ac}} = 1 - \left(\frac{2}{3}\frac{F_{i_{crit}}}{\overline{F_i}}\right)^2, 0 \le \frac{A_{trans}}{A_{ac}} < 1; \tag{9}$$

Similarly, the equivalent radius of the zone in full contact a_{trans} can be found as:

$$a_{trans} = a_{ac}\,(A_{trans}/A_{ac})^{1/2} \tag{10}$$

The mean pressures in full contact and asperity contact regions, $\overline{p}_{trans}$ and $\overline{p}_{asp}$ respectively, can be calculated through integration of the Hertzian pressure distribution equation over the corresponding areas:

$$\overline{p}_{trans} = \frac{1}{\pi a_{trans}^2}\int_0^{a_{trans}} \frac{3}{2}\overline{p}\sqrt{1-\frac{r^2}{a_{ac}^2}} * 2\pi r\, dr \tag{11}$$

$$\overline{p}_{asp} = \frac{1}{\pi (a_{ac}^2 - a_{trans}^2)}\int_{a_{trans}}^{a_{ac}} \frac{3}{2}\overline{p}\sqrt{1-\frac{r^2}{a_{ac}^2}} * 2\pi r\, dr \tag{12}$$

3.3. Asperity Forces

The critical force per asperity $F_{i_{crit}}$ can be calculated if material properties, asperity dimensions and normal load F_{crit}, at which transition starts, are known. If the Hertzian theory is applied to the micro-contact at a point when combined micro-displacement δ equals the asperity height h_{asp}, the following set of equations can be written:

$$\begin{cases} F_{i_{crit}} = \frac{3}{2}\overline{F_i} = \frac{3}{2}\frac{F_{crit}}{A_{ac}} * \lambda^2; \\ \delta = h_{asp} = \left(\frac{9}{16}\frac{F_{i_{crit}}^2}{E_1^{*2} R_{asp}}\right)^{\frac{1}{3}}. \end{cases} \tag{13}$$

R_{asp} is the radius of an individual asperity; E_1^* is a reduced Young's modulus for micro contact and equals $E_1^* = 1/((1-\upsilon_{smc}^2)/E_{smc} + (1-\upsilon_m^2)/E_m)$, where υ_{smc} and E_{smc} are a Poisson's ratio and an effective Young's modulus of the skin in micro-scale contact respectively. Therefore, the dependency of the skin effective elastic modulus and the normal load, at which transition starts, can be expressed after the simplification as:

$$F_{crit} = \frac{8}{9}\frac{\sqrt{h_{asp}^3 R_{asp}}}{\lambda^2} * A_{ac} * E_1^* \tag{14}$$

While simplified Hertzian contact can be used as a first approximation, it cannot be applied for precise calculations due to the high asperity density and contribution of the compressive stresses from the surrounding surface features. This approach overestimates the effective elastic modulus and the normal forces required for the contact transition to happen.

The problem of stress distribution at any point in a semi-infinite isotropic and homogeneous elastic half-space was solved by Boussinesq [35] and is widely used in numerical contact models [36–38]. Therefore, calculation of stresses on the micro-scale is performed by a numerical half-space contact model assuming the skin as an ideal flat elastic surface. The asperity height data obtained from confocal microscopy is used as a countersurface, thus representing microroughness which includes deviations in geometry. The simulation is performed in iterations changing the elastic skin modulus until the normal force, at which transition occurs in experiments, does not fit the normal force used in simulation. The point at which the contact transition happens is defined as the point when the total micro-displacement equals the mean asperity height. After the solution is found, $F_{i_{crit}}$ is calculated as the force

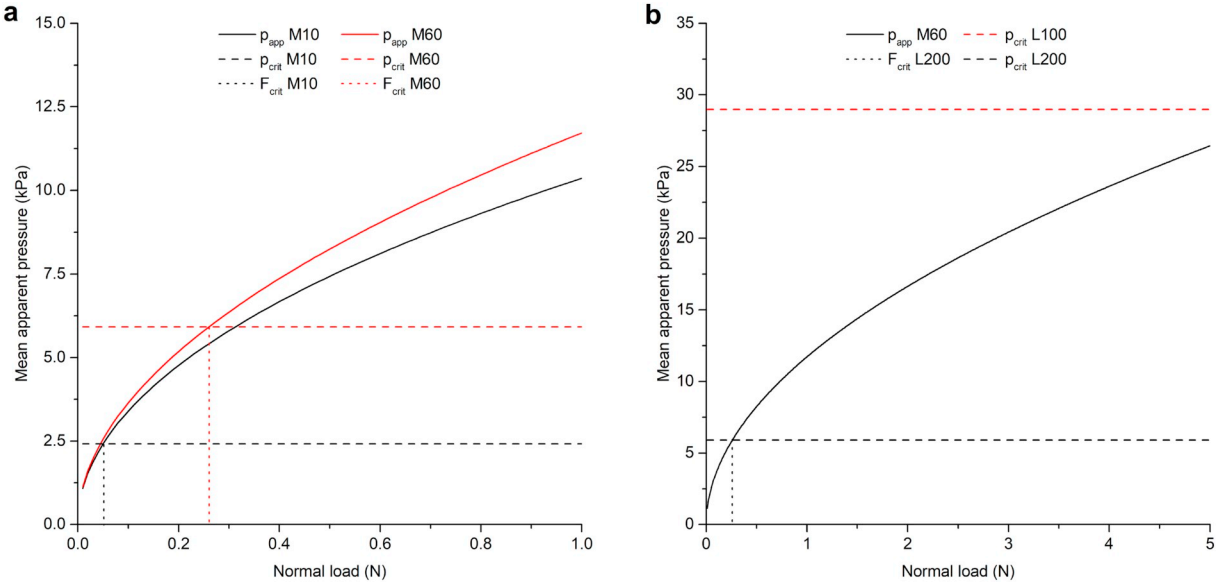

Fig. 4. Relationship between mean apparent pressure, critical mean pressure and critical normal load for the texture L200 (a) and the material M60 (b).

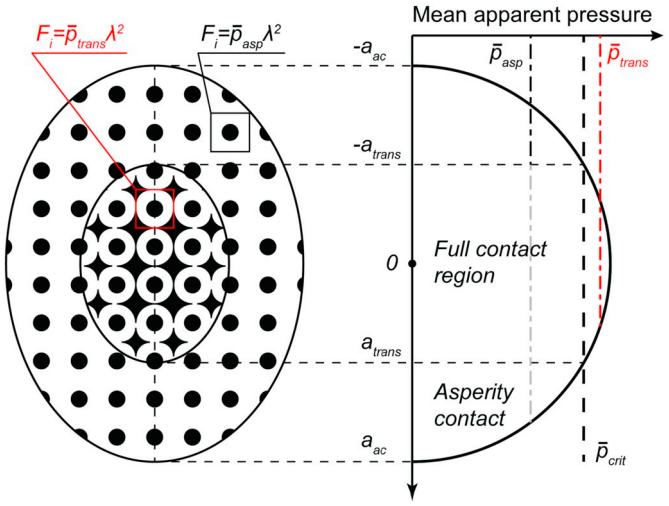

Fig. 5. Schematic representation of the contact states, apparent mean pressures and asperity forces.

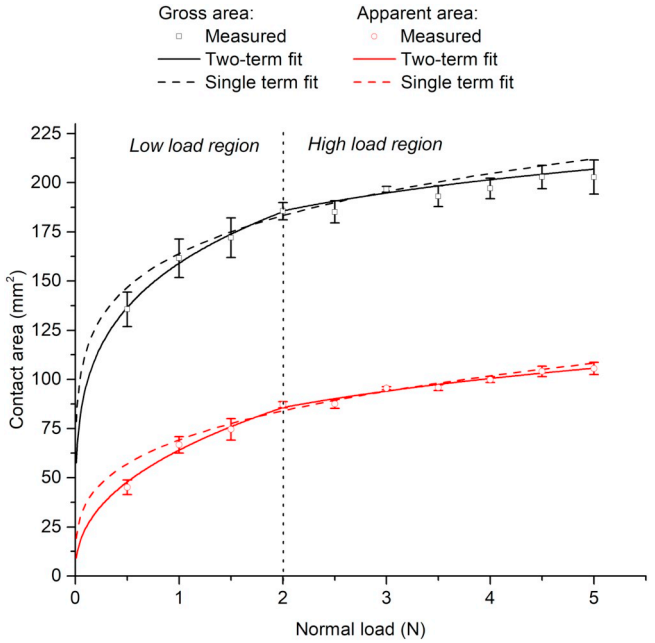

Fig. 6. Experimental gross and apparent contact areas.

Fig. 7. Typical example of the finger pad elliptic fit and apparent contact area after image filtering at 2 N normal load.

acting on an individual asperity. The corresponding mean apparent contact pressure required for the contact transition can be found as $\bar{p}_{crit} = 2/3 * F_{icrit}/\lambda^2$.

A graphical representation of the proposed approach is shown in Fig. 4 and illustrates the dependency similar to Eq. (14). Fig. 4a shows an example of calculations performed for the constant skin elastic modulus, surface texture L200 and two materials. Contact transition occurs when the mean apparent contact pressure reaches its critical value at the normal load F_{crit}. Both of these values can be obtained experimentally. In turn, the critical mean pressure $\bar{p}_{crit}$ for a given texture varies as a function of the effective elastic modulus E_1^* and, if the counter material elastic modulus is known, effective skin elasticity can be estimated. Moreover, if the Young's modulus of the skin is assumed constant between the measurements, relative values of the transition force F_{crit} for various materials can characterize the change in the finger pad ridge contact area. The comparison for the same skin elasticity and material, but different texture is shown on Fig. 4b. In this case, $\bar{p}_{crit}$ varies as a function of texture dimensions and limits the maximum mean pressure for the L100 texture. Therefore, finger pad skin remains in an asperity-only contact state.

With the obtained critical force values and elastic modulus the numerical half-space simulations are performed to calculate the real contact area for the three cases: no contact transition at $F_i = \bar{F}_i$, point of transition at $F_i = F_{i_{crit}}$ and full contact, where the force acting on the asperity inside the transition zone equals $F_i = \bar{p}_{trans} * \lambda^2$ and outside $F_i = \bar{p}_{asp} * \lambda^2$ as calculated by Eqs. (11) and (12). Resulting contact areas are multiplied by the corrected apparent contact area and summed up by the ratio A_{trans}/A_{ac} calculated according to Eq. (9). Schematic representation of the contact regions, average apparent pressures and asperity forces is shown in Fig. 5.

4. Results and Discussion

4.1. Gross and Apparent Contact Area

Gross and apparent contact area measurements are shown in Fig. 6 with the typical images obtained from the digital scanner presented in Fig. 7. The data can be fitted to power law functions: $A_g = k_g F^{m_g}$ for the gross and $A_a = k_a F^{m_a}$ for the apparent contact area, where k is a load coefficient and m is a load index. Best power fits give the coefficients of 164 and 69 and the load indices of 0.16 and 0.28 for the finger pad and ridge contact areas respectively. However, the quality of such fits is relatively poor for both low and high normal loads, where the measured contact area shows lower values.

Recently, Dzidek et al. [27] explained the nature of such behaviour by the change in elastic modulus of the finger pad with displacement. At low normal loads the stiffer SC layer significantly contributes to the effective Young's modulus, but with an increase of displacement its influence reduces, and elastic modulus becomes governed by the dermis. At high normal loads the elastic modulus of a finger pad rises again as it becomes compressed against a *distal phalanx* bone. At this point further contact area development becomes constrained by the skin stress-strain behaviour.

Liu et al. [39] reported similar observations and proposed a two term function which separates two normal load regions. Following their approach, gross contact area fit develops with coefficients of 159 and 171 and exponents of 0.22 and 0.12 for low and high normal load regions respectively. The apparent contact area increases slightly faster, with the corresponding coefficients of 64 and 73 and exponents of 0.42 and 0.23, which leads to the gradual increase of the ridge to gross contact ratio up to 0.52 at 5 N.

Reported exponents for the apparent contact area of the index finger pad in literature vary significantly from 0.2 to 0.7 [27,39–41] and depend on the finger pad inclination angle, environmental conditions and personal differences. Moreover, the calculated coefficients are influenced by the image processing and selected threshold for the ink

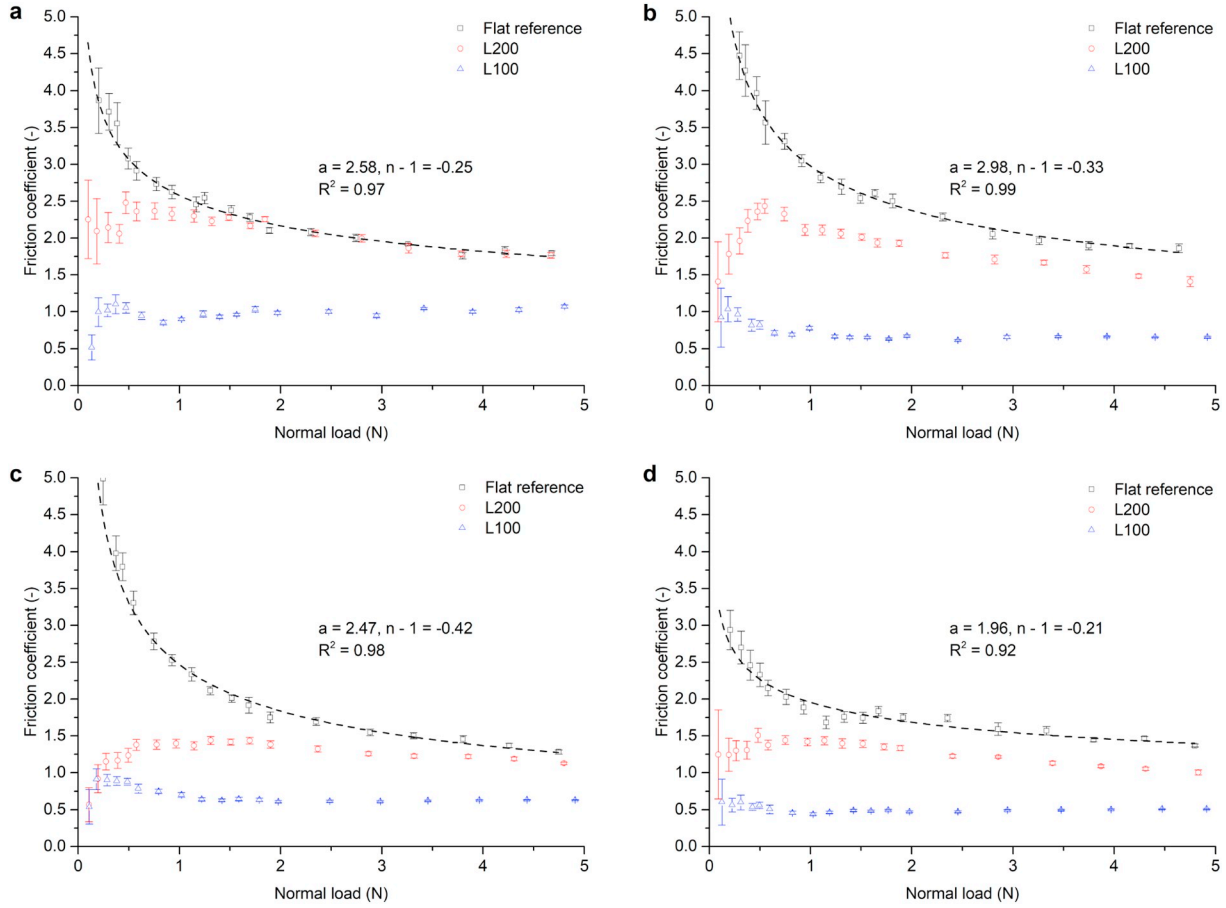

Fig. 8. Calculated friction coefficients grouped by rubber grades: M10 (a), M30 (b), M40 (c), M60 (d).

print or digital scanner measurement methods. Therefore, absolute values cannot be compared with other reports.

4.2. Texture and Sample Hardness Influence

Fig. 8 shows calculated friction coefficients for the four materials tested. For the smooth reference surfaces, the coefficient of friction reduces with an increase of the normal load and follows a commonly observed power law function: $\mu \propto F^{n-1}$, with the n of 0.75, 0.67, 0.58 and 0.79 for all the rubber grades from the softest to the hardest respectively. For an elastic material the exponent n shall decrease with the rise in the rubber Young's modulus due to the reduction in contact area and hysteresis friction component. However, the results for the M60 sample show a contradicting behaviour.

Moreover, the hardest non-textured sample shows a distinctive local increase in friction at 1.8 N, which breaks the consistent power trend and reduces the coefficient of determination. Small deviations for other reference samples can also be observed in the region between 1 and 2 N. The contacting surfaces are not ideally smooth, and their contact compliance is directly related to the material hardness. Therefore, the observed local peaks are possibly connected to the deformation of the asperities and transition to the full contact state. It implies that the power function fitted to the hardest reference sample cannot be used to estimate the apparent contact area development.

All L200 textures show a completely different trend as compared to the reference samples. At low normal loads the coefficient of friction is significantly reduced, but it rises quickly with a further increase of normal load, coming to its maximum around 0.8 N. This peak is followed by a steady decline with the values nearly reaching the friction results of the non-textured samples. Similar bell-curved shapes of the friction coefficient were reported previously as the influence of moisture [22,42,43]. Tomlinson et al. [42] concluded that an increase in friction comes mainly from the rise in the real contact area as skin softens.

Three contact cases can be considered for the skin sliding against textured surfaces. Initially the skin is supported only by the texture asperities, which reduce the real contact area. With an increase of the normal load, a combined micro displacement of skin and asperities will reach the asperity height value, leading to the contact transition state. This case can be characterized by a rapid growth of the real contact area and therefore drop in the mean pressure. Once the contact stabilizes and reaches a full contact state, the mean pressure starts to gradually rise again.

The high density L100 texture shows significantly lower values of the friction coefficient (between 0.5 and 1), which remain almost constant for the entire range of the tested normal loads. Only the softest high-density texture demonstrates a linear increase in the coefficient of friction, which can be connected to the predominant deformation of the texture asperities and higher hysteresis friction losses due to the larger material displacement [44].

A slight increase in the friction coefficient can be observed for all L100 textures at the normal loads around 0.3–0.5 N. It diminishes with an increase in sample hardness and can be explained by material deformation. As discussed earlier, the finger pad Young's modulus reduces with displacement at low normal loads [27]. Consequently, the initial increase in gross and apparent contact area on a soft material is achieved mainly by its deformation, while finger pad displacement remains relatively low.

With an increase in material hardness, the coefficient of friction generally decreases (Fig. 9). The observed deviation in the relative

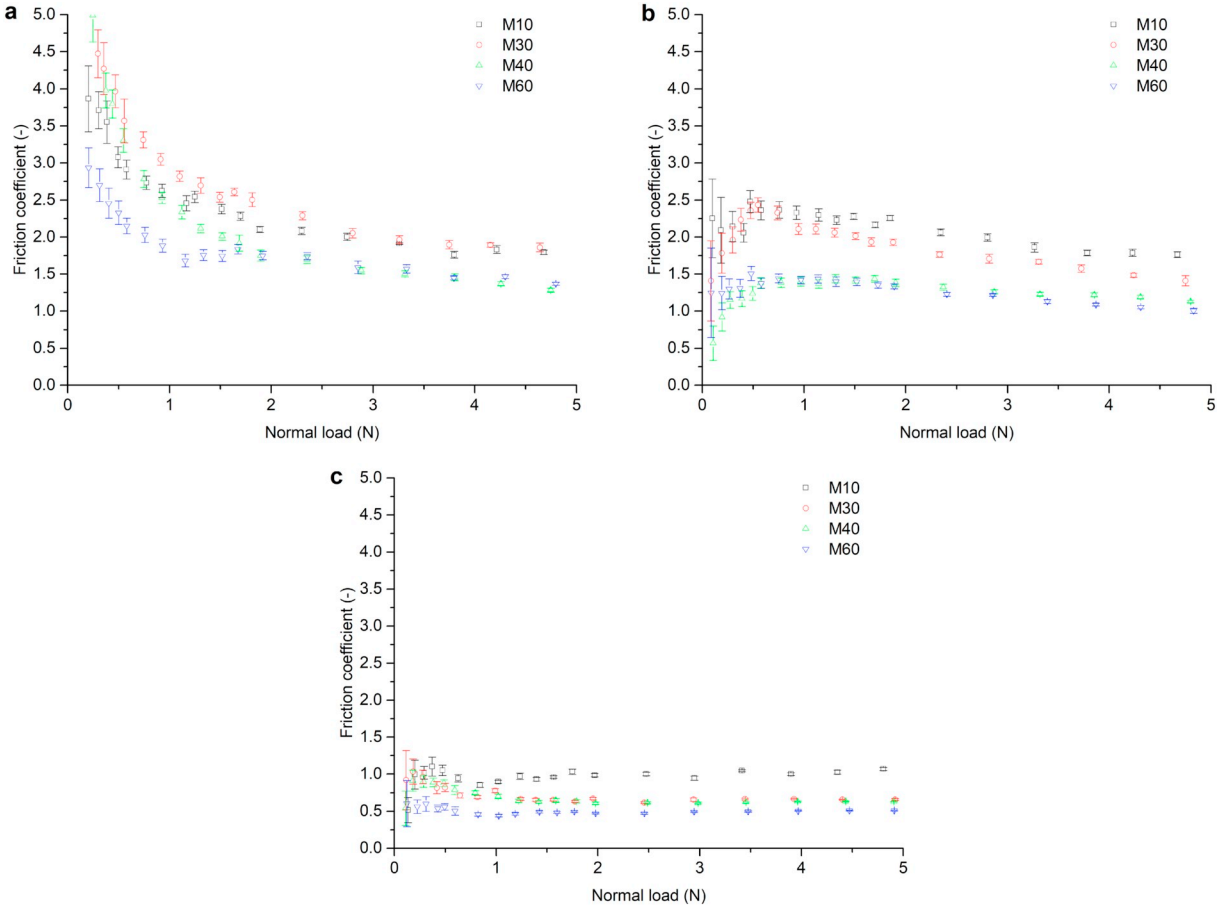

Fig. 9. Calculated friction coefficient grouped by surface texture: flat reference (a), L200 (b) and L100 (c).

Table 3
Calculated Young's modulus of the skin at the micro-scale and micro-deformations at the point of transition for the L200 texture.

Material	M10	M30	M40	M60
Calculated Young's modulus [MPa]	0.5	0.2	0.25	0.2
SC deformation [μm]	8.7	22.9	25.4	29.1
Asperity deformation [μm]	21.2	6.1	4.8	2.5

friction values for the M30 reference sample in Fig. 9a can be explained by the lower surface roughness. Small variations of the relative friction values are assumed to arise from the minor changes in stratum corneum hydration level during a given measurement series.

4.3. Modelling Results

Friction can be approximated by the two-term model expression (1), where the adhesion term can be described as a product of interfacial shear strength and real contact area $F_{adh} = \tau A_r$. Adams et al. [7] proposed that interfacial shear strength can be expressed as $\tau = \tau_0 + \alpha \overline{p}_r$ accounting for the organic film in the dry contact, where τ_0 is an intrinsic shear strength, α is a pressure coefficient and $\overline{p}_r$ is a mean real pressure. A hysteresis component arising from an elastic material deformation can be described as [44]:

$$F_{def} = \beta \left(\frac{9}{128 R_e}\right)^{\frac{2}{3}} \left(\frac{F^4}{E_0^*}\right)^{\frac{1}{3}} \tag{15}$$

where β is viscoelastic hysteresis loss fraction, R_e is the equivalent finger pad radius, E_0^* is the effective Young's modulus in macro contact and F is applied normal load. Deformation of the skin and asperities on the microscale is assumed to be insignificant, considering low asperity heights. Therefore, the total coefficient of friction can be estimated as:

$$\mu_{tot} = \mu_{adh} + \mu_{def} = \frac{\tau_0 A_r}{F} + \alpha + \beta \left(\frac{9}{128 R_e}\right)^{\frac{2}{3}} \left(\frac{F}{E_0^*}\right)^{\frac{1}{3}} \tag{16}$$

The approach described in Section 3 was used to estimate an effective elastic modulus of the skin at the micro-scale and to calculate real contact areas. Finger pad equivalent radius R_e was estimated as 11 mm, while Poisson's ratios for the skin and silicone rubber grades were assumed to be equal 0.5 and 0.49 respectively [5,45,46]. With the curve fits of the apparent contact area obtained from a fingerprint scanner the elastic modulus in the range of 0.2–0.5 MPa was calculated (Table 3). Nonetheless, the same relative position of the inverse pressure peaks at the observed normal load of 0.8 N cannot be obtained. Furthermore, the measured exponents of 0.42 and 0.23 are too low compared to the power of 0.58 obtained from the experiment.

Clearly, the simple approximations and assumptions described by Eqs. (3) and (4) cannot be applied to estimate gross and apparent contact areas for elastomers. Experimental observations suggest that finger pad elastic modulus should be considered as a function of displacement and gross contact area [27,39]. Compared to the rigid materials, gross contact area with elastomers will develop faster, thus increasing the depth of the maximum subsurface stresses as described by Hertzian contact. It will reduce the influence of stratum corneum on finger pad Young's modulus at low normal loads. The constraint arising from *distal phalanx* bone and skin strain will also be less pronounced, due to the reduced relative deformation of the finger pad and higher rubber compliance. Therefore, with the reduction of the counter-material elastic modulus, the contact area development trend shown in Fig. 6 will change at greater normal load and the two-term evolution

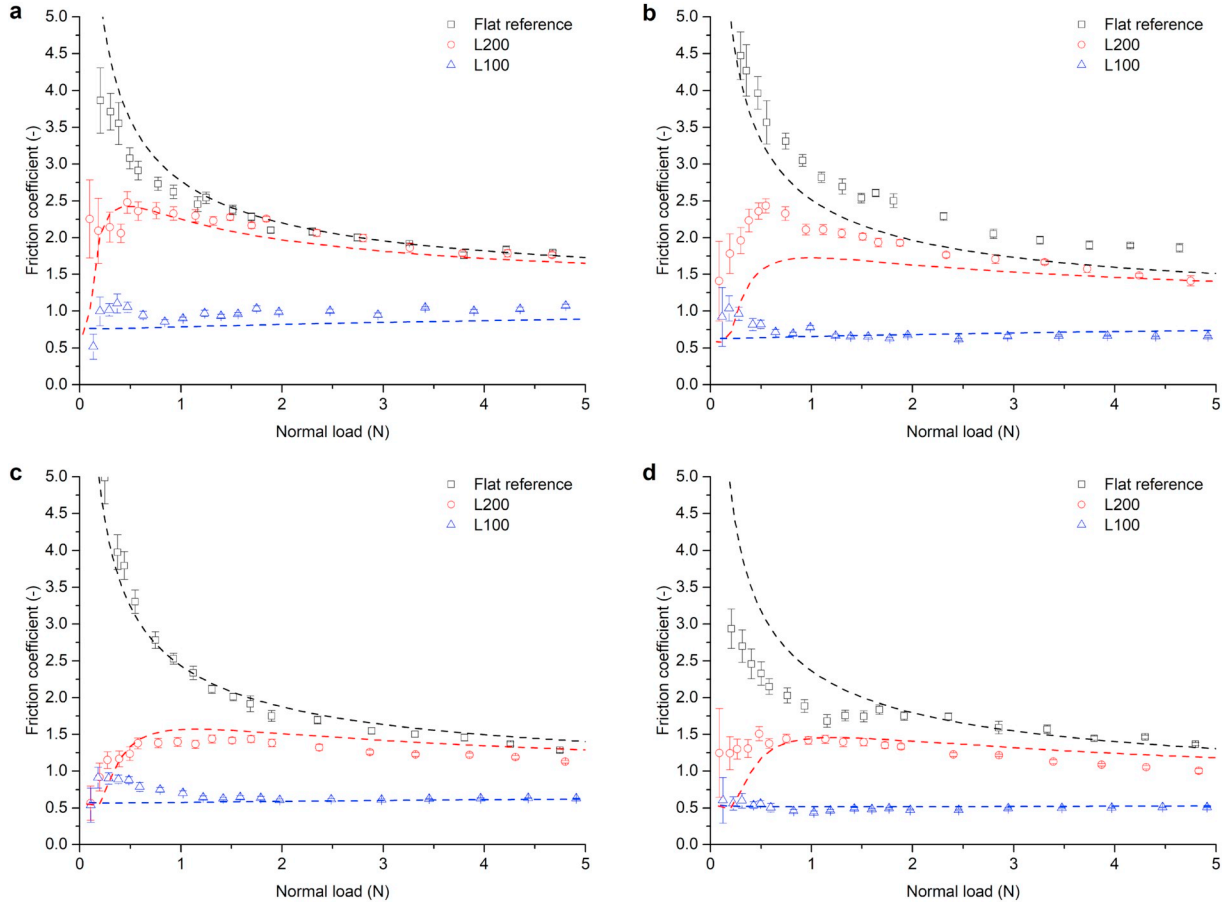

Fig. 10. Closest model fit for the friction coefficient measurements grouped by rubber grades: M10 (a), M30 (b), M40 (c), M60 (d).

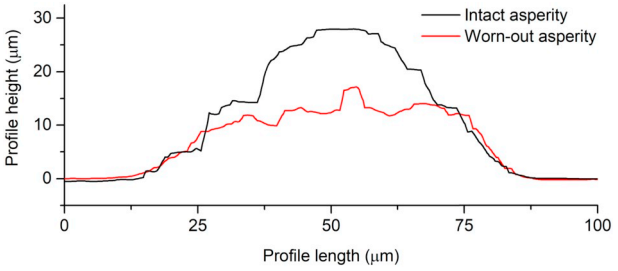

Fig. 11. Asperity surface profile wear for the L200 M60 sample.

can take the form of the one-term power law fit.

The obtained elastic modulus is of the same order and comparable to optical coherence tomography measurements and values calculated from the fingerprint ridge deformations [27,46]. However, the calculated values are significantly smaller than typically reported from *in-vitro* indentation measurements, where the values vary from 0.6 MPa to 1 GPa [23,25]. Pailler-Mattei et al. [23] reported the reduction of the SC Young's modulus from 1 GPa to 1 MPa with an increase of the penetration depth from 10 nm to about 4 μm on isolated skin samples. If the stratum corneum elasticity continues to decrease with further deformation, the calculated values become feasible, considering, that the indentation depths in the current work are much higher (see Table 3). Moreover, it can provide another possible explanation for the higher Young's modulus obtained for the M10 sample. Such behaviour can be explained by anisotropic SC structure and increase of its moisture content with depth, which makes the skin more compliant at higher displacements.

The closest model fit was found for the $A_a \approx 85F^{0.49}$ with corresponding skin elastic modulus of 0.2 MPa for L200 and reference samples and with 0.4 MPa for L100 texture. Such an exponent for the apparent contact area seems reasonable considering the lowest experimental friction coefficient exponent n-1 = −0.42. While it does not allow for analysing of the results quantitatively, the relative values still explain the observed friction behaviour, as the real contact area remains directly proportional to the apparent contact area. The intrinsic interfacial shear strength τ_0 was considered constant for all the tested materials, while the hysteresis coefficient was varied. The curve fits were obtained with a pressure coefficient $\alpha = 0.35$ and presented in Fig. 10. While the friction coefficient can be fitted relatively well, it is impossible to achieve a good result in both low and high normal load regions for various materials by using a single term power law.

4.4. Surface Wear

Surface wear observed on the tested surfaces did not exceed the standard deviation of the texture dimensions. The only exception was for the L200 M60 samples, where approximately 35% of the asperities were damaged by tear. An example wear profile of such an asperity is presented in Fig. 11. While the wear can be considered gradual and the full contact is achieved at relatively low normal loads, influence of wear on friction measurements is considered insignificant. According to material specification the tensile strength for the M60 is 2.7 MPa, which is the lowest among other materials. The analysis of the stress distribution could allow to estimate shear and tensile forces acting on asperity, however, it is beyond the scope of the current work.

5. Conclusions

- Transition from asperity-only to full contact was shown through the friction measurements. The distinctive contact transition peak is expected to become less prominent with increase of sample or skin elastic modulus, reduction of texture spacing and rise in sub-texture roughness.
- The proposed method can be used for the rough estimation of skin elasticity, real contact area and texture design, if the apparent contact area development is accurately predicted. The model is limited to dry finger pad contact and restricted to the textures with lateral spacings below the fingerprint ridge width and relatively small heights as compared to the thickness of the stratum corneum.
- The values of the effective skin Young's modulus estimated with the proposed empirical approach vary between 0.2 and 0.5 MPa. The obtained results are slightly higher but of the same order as values calculated from fingerprint ridge deformation models and more direct optical coherence tomography measurements.
- Experimental results with elastomers show significantly higher exponents for the apparent contact area development with increase of normal load than estimated by Hertzian contact. It is expected that high counter-surface compliance reduces the influence of the constraints arising from stratum corneum and *distal phalanx* bone at low and high normal loads respectively.

Ethical Approval

All procedures performed in the current studies involving human participant were in accordance with the ethical standards of the institutional and/or national research committee and with the 1964 Helsinki declaration and its later amendments or comparable ethical standards. The subject provided a written informed consent. None of the experiments were invasive or harmful physiologically or psychologically.

Acknowledgements

This work was supported by INTERREG V-A Deutschland – Nederland program MOVERO under the project number 142091.

Appendix A. Supplementary data

Supplementary data to this article can be found online at https://doi.org/10.1016/j.biotri.2019.100097.

References

[1] T. Yoshioka, S.J. Bensmaïa, J.C. Craig, S.S. Hsiao, Texture perception through direct and indirect touch: an analysis of perceptual space for tactile textures in two modes of exploration, Somatosens. Mot. Res. (2007), https://doi.org/10.1080/08990220701318163.

[2] L. Skedung, K. Danerlöv, U. Olofsson, C. Michael Johannesson, M. Aikala, J. Kettle, M. Arvidsson, B. Berglund, M.W. Rutland, Tactile perception: finger friction, surface roughness and perceived coarseness, Tribol. Int. 44 (2011) 505–512, https://doi.org/10.1016/j.triboint.2010.04.010.

[3] L.E.M. Grierson, H. Carnahan, Manual exploration and the perception of slipperiness, Percept. Psychophys. 68 (2006) 1070–1081, https://doi.org/10.3758/BF03193710.

[4] R. Fagiani, F. Massi, E. Chatelet, Y. Berthier, A. Akay, Tactile perception by friction induced vibrations, Tribol. Int. 44 (2011) 1100–1110, https://doi.org/10.1016/j.triboint.2011.03.019.

[5] R. Fagiani, M. Barbieri, A contact mechanics interpretation of the duplex theory of tactile texture perception, Tribol. Int. 101 (2016) 49–58, https://doi.org/10.1016/j.triboint.2016.03.031.

[6] G. Robles-De-La-Torre, V. Hayward, Force can overcome object geometry in the perception of shape through active touch, Nature 412 (2001) 445–448, https://doi.org/10.1038/35086588.

[7] M.J. Adams, B.J. Briscoe, S.A. Johnson, Friction and lubrication of human skin, Tribol. Lett. 26 (2007) 239–253, https://doi.org/10.1007/s11249-007-9206-0.

[8] S.A. Johnson, D.M. Gorman, M.J. Adams, B.J. Briscoe, The friction and lubrication of human stratum corneum, Tribol. Ser. 25 (1993) 663–672, https://doi.org/10.1016/S0167-8922(08)70419-X.

[9] S. Derler, L.C. Gerhardt, A. Lenz, E. Bertaux, M. Hadad, Friction of human skin against smooth and rough glass as a function of the contact pressure, Tribol. Int. 42 (2009) 1565–1574, https://doi.org/10.1016/j.triboint.2008.11.009.

[10] K. Duvefelt, U. Olofsson, C.M. Johannesson, L. Skedung, Model for contact between finger and sinusoidal plane to evaluate adhesion and deformation component of friction, Tribol. Int. 96 (2016) 389–394, https://doi.org/10.1016/j.triboint.2014.12.020.

[11] S. Derler, G.M. Rotaru, Stick-slip phenomena in the friction of human skin, Wear 301 (2013), https://doi.org/10.1016/j.wear.2012.11.030.

[12] S.E. Tomlinson, R. Lewis, M.J. Carré, The effect of normal force and roughness on friction in human finger contact, Wear 267 (2009) 1311–1318, https://doi.org/10.1016/j.wear.2008.12.084.

[13] S.E. Tomlinson, M.J. Carré, R. Lewis, S.E. Franklin, Human finger contact with small, triangular ridged surfaces, Wear 271 (2011) 2346–2353, https://doi.org/10.1016/j.wear.2010.12.055.

[14] M.A. Darden, C.J. Schwartz, Skin tribology phenomena associated with reading braille print: the influence of cell patterns and skin behavior on coefficient of friction, Wear 332–333 (2015) 734–741, https://doi.org/10.1016/j.wear.2014.12.053.

[15] S. Zhang, X. Zeng, D.T.A. Matthews, A. Igartua, E. Rodriguez–Vidal, J.C. Fortes, E. van der Heide, Texture design for light touch perception, Biosurface Biotribology 3 (2017) 25–34, https://doi.org/10.1016/j.bsbt.2017.02.002.

[16] M.A. Masen, A systems based experimental approach to tactile friction, J. Mech. Behav. Biomed. Mater. 4 (2011) 1620–1626, https://doi.org/10.1016/j.jmbbm.2011.04.007.

[17] J. van Kuilenburg, M.A. Masen, M.N.W. Groenendijk, V. Bana, E. van der Heide, An experimental study on the relation between surface texture and tactile friction, Tribol. Int. 48 (2012) 15–21, https://doi.org/10.1016/j.triboint.2011.06.003.

[18] J. van Kuilenburg, M.A. Masen, E. van der Heide, The role of the skin microrelief in the contact behaviour of human skin: contact between the human finger and regular surface textures, Tribol. Int. 65 (2013) 81–90, https://doi.org/10.1016/j.triboint.2012.11.024.

[19] C. Merle, A. Baillet-Guffroy, Physical and chemical perturbations of the supramolecular organization of the stratum corneum lipids: in vitro to ex vivo study, Biochim. Biophys. Acta Biomembr. 1788 (2009) 1092–1098, https://doi.org/10.1016/j.bbamem.2009.02.010.

[20] H. Fruhstorfer, U. Abel, C.D. Garthe, A. Knüttel, Thickness of the stratum corneum of the volar fingertips, Clin. Anat. 13 (2000) 429–433, https://doi.org/10.1002/1098-2353(2000)13:6<429::AID-CA6>3.0.CO;2-5.

[21] M.J. Adams, S.A. Johnson, P. Lefèvre, V. Lévesque, V. Hayward, T. André, J.-L. Thonnard, Finger pad friction and its role in grip and touch, J. R. Soc. Interface 10 (2013) 20120467, https://doi.org/10.1098/rsif.2012.0467.

[22] X. Liu, Z. Lu, R. Lewis, M.J. Carré, S.J. Matcher, Feasibility of using optical coherence tomography to study the influence of skin structure on finger friction, Tribol. Int. 63 (2013) 34–44, https://doi.org/10.1016/j.triboint.2012.08.020.

[23] C. Pailler-Mattei, S. Pavan, R. Vargiolu, F. Pirot, F. Falson, H. Zahouani, Contribution of stratum corneum in determining bio-tribological properties of the human skin, Wear. 263 (2007) 1038–1043, https://doi.org/10.1016/j.wear.2007.01.128.

[24] Y. Yuan, R. Verma, Measuring microelastic properties of stratum corneum, Colloids Surf. B: Biointerfaces 48 (2006) 6–12, https://doi.org/10.1016/j.colsurfb.2005.12.013.

[25] M. Geerligs, L. van Breemen, G. Peters, P. Ackermans, F. Baaijens, C. Oomens, In vitro indentation to determine the mechanical properties of epidermis, J. Biomech. 44 (2011) 1176–1181, https://doi.org/10.1016/j.jbiomech.2011.01.015.

[26] J. van Kuilenburg, M.A. Masen, E. van der Heide, Contact modelling of human skin: what value to use for the modulus of elasticity? Proc. Inst. Mech. Eng. Part J. Eng. Tribol. 227 (2012) 349–361, https://doi.org/10.1177/1350650112463307.

[27] B.M. Dzidek, M.J. Adams, J.W. Andrews, Z. Zhang, S.A. Johnson, Contact mechanics of the human finger pad under compressive loads, J. R. Soc. Interface 14 (2017) 20160935, https://doi.org/10.1098/rsif.2016.0935.

[28] A. Abdouni, M. Djaghloul, C. Thieulin, R. Vargiolu, C. Pailler-Mattei, H. Zahouani, Biophysical properties of the human finger for touch comprehension: Influences of ageing and gender, R. Soc. Open Sci 4 (2017), https://doi.org/10.1098/rsos.170321.

[29] P. Cornuault, L. Carpentier, M. Bueno, J. Cote, G. Monteil, Influence of physico-chemical, mechanical and morphological fingerpad properties on the frictional distinction of sticky/slippery surfaces, J. R. Soc. Interface 12 (2015) 20150495, https://doi.org/10.1098/rsif.2015.0495.

[30] S. Zhang, A. Rodriguez Urribarri, M. Morales Hurtado, X. Zeng, E. van der Heide, The role of the sliding direction against a grooved channel texture on tool steel: an experimental study on tactile friction, Int. J. Solids Struct. 56 (2015) 53–61, https://doi.org/10.1016/j.ijsolstr.2014.12.005.

[31] A.C. Rodriguez Urribarri, E. van der Heide, X. Zeng, M.B. de Rooij, Modelling the static contact between a fingertip and a rigid wavy surface, Tribol. Int. 102 (2016) 114–124, https://doi.org/10.1016/j.triboint.2016.05.028.

[32] M. Klaassen, D.J. Schipper, M.A. Masen, Influence of the relative humidity and the temperature on the in-vivo friction behaviour of human skin, Biotribology. 6 (2016) 21–28, https://doi.org/10.1016/j.biotri.2016.03.003.

[33] U. Heinrich, U. Koop, M.C. Leneveu-Duchemin, K. Osterrieder, S. Bielfeldt, C. Chkarnat, J. Degwert, D. Häntschel, S. Jaspers, H.P. Nissen, M. Rohr, G. Schneider, H. Tronnier, Multicentre comparison of skin hydration in terms of physical-, physiological- and product-dependent parameters by the capacitive method (Corneometer CM 825), Int. J. Cosmet. Sci. (2003), https://doi.org/10.1046/j.1467-2494.2003.00172.x.

[34] L.R. Manfredi, H.P. Saal, K.J. Brown, M.C. Zielinski, J.F. Dammann, V.S. Polashock, S.J. Bensmaia, Natural scenes in tactile texture, J. Neurophysiol. 111 (2014), https://doi.org/10.1152/jn.00680.2013.
[35] K.L. Johnson, Contact Mechanics, Cambridge University Press, Cambridge, 1985.
[36] G.K. Nikas, Boussinesq-Cerruti functions and a simple technique for substantial acceleration of subsurface stress computations in elastic half-spaces, Proc. Inst. Mech. Eng. Part J. Eng. Tribol. 220 (2006) 19–28, https://doi.org/10.1243/13506501JET125.
[37] W.W. Chen, Q.J. Wang, A numerical static friction model for spherical contacts of rough surfaces, influence of load, material, and roughness, J. Tribol. 131 (2009) 021402, , https://doi.org/10.1115/1.3063814.
[38] J. Cesbron, H.P. Yin, F. Anfosso-Lédée, D. Duhamel, D. Le Houédec, Z.Q. Feng, Numerical and experimental study of multi-contact on an elastic half-space, Int. J. Mech. Sci. 51 (2009) 33–40, https://doi.org/10.1016/j.ijmecsci.2008.11.003.
[39] X. Liu, M.J. Carré, Q. Zhang, Z. Lu, S.J. Matcher, R. Lewis, Measuring contact area in a sliding human finger-pad contact, Skin Res. Technol. 24 (2018) 31–44, https://doi.org/10.1111/srt.12387.
[40] T. Soneda, K. Nakano, Investigation of vibrotactile sensation of human fingerpads by observation of contact zones, Tribol. Int. 43 (2010) 210–217, https://doi.org/10.1016/j.triboint.2009.05.016.
[41] H.T. Lin, T.F. Hong, W.L. Li, Grip performance affected by water-induced wrinkling of fingers, Tribol. Lett. 58 (2015) 1–9, https://doi.org/10.1007/s11249-015-0515-4.
[42] S.E. Tomlinson, R. Lewis, X. Liu, C. Texier, M.J. Carré, Understanding the friction mechanisms between the human finger and flat contacting surfaces in moist conditions, Tribol. Lett. 41 (2011) 283–294, https://doi.org/10.1007/s11249-010-9709-y.
[43] T. André, P. Lefèvre, J.L. Thonnard, A continuous measure of fingertip friction during precision grip, J. Neurosci. Methods 179 (2009) 224–229, https://doi.org/10.1016/j.jneumeth.2009.01.031.
[44] J.A. Greenwood, H. Minshall, D. Tabor, Hysteresis losses in rolling and sliding friction, Proc. R. Soc. A Math. Phys. Eng. Sci. 259 (1961) 480–507, https://doi.org/10.1098/rspa.1961.0004.
[45] J. Ilg, S.J. Rupitsch, A. Sutor, R. Lerch, Determination of dynamic material properties of silicone rubber using one-point measurements and finite element simulations, IEEE Trans. Instrum. Meas. 61 (2012) 3031–3038, https://doi.org/10.1109/TIM.2012.2203449.
[46] X. Liang, S.A. Boppart, Biomechanical properties of in vivo human skin from dynamic optical coherence elastography, IEEE Trans. Biomed. Eng. 57 (2010) 953–959, https://doi.org/10.1109/TBME.2009.2033464.